Originals

Experiments in Fluids 21 (1996) 315–324 © Springer-Verlag 1996

An experimental study of viscous vortex rings

M. Dziedzic, H. J. Leutheusser

Abstract The work focuses on the problem of stability and viscous decay of single vortex rings. A tentative classification scheme is proposed for vortex rings which is based on extensive hot-wire measurements of velocity in the ring core and wake, and flow visualization, viz. laminar, wavy, turbulence-producing, and turbulent. Prediction of vortex ring type is shown to be possible, at least approximately, based on the vortex ring Reynolds number alone. Linear growth rates of ring diameter with time are observed for all types of vortex rings, with different growth rates occurring for laminar and turbulent vortex rings. Data on the viscous decay of vortex rings are used to provide experimental confirmation of the accuracy of Saffman's equation for the velocity of propagation of a vortex ring.

1 Introduction

Vortex motions are fast swirling movements of fluids. They encompass a vast spectrum of relatively ordered phenomena which range from the hurricanes, typhoons and tornadoes of meteorology, and the whirlpools in kitchen and bathroom sinks, to the multitude of eddies characterizing turbulent motion.

Of the many forms in which a vortex may occur, the ringlike shape is outstanding. Once created, it is self-contained, automotive and quite longevous. Because of this, the vortex ring has found some use as a mass transfer "vehicle" in environmental engineering. On a more fundamental level, interacting rings are suspected of forming the building blocks of fluid turbulence.

Much has been studied about these interactions, and yet much remains to be unveiled. Thus, basic points such as growth and decay of a single viscous vortex ring still need to be elucidated and these are the subject of the present work. Moreover, a classification scheme of vortex rings is sought in order to refine the differentiation between the various types.

Received: 14 August 1995/Accepted: 22 February 1996

M. Dziedzic, H. J. Leutheusser
Department of Mechanical and Industrial Engineering,
University of Toronto, 5 King's College Road,
Toronto, Canada - M5S 3G8

The work reported herein is supported through a grant of the Natural Sciences and Engineering Research Council of Canada. Special thanks are due to CAPES (Brazil) for the award of a scholarship to the senior author.

2 Background Review

Figure 1 schematically depicts a vortex ring, defining the principal terminology employed in the following. The circulation around the core is Γ, the self-induced velocity of propagation is U, the diameter of the ring is D, its radius is $R=D/2$, and the radius of the core is r_c. The cylindrical coordinate system employed comprises (x, r, Φ). The ring induces velocity components (u, v) in the surrounding fluid at location $r'=(x^2+r^2)^{1/2}$, and the velocity U upon itself.

In the usual case, a vortex ring is formed by the rollup of a cylindrical vortex sheet created by impulsive ejection of fluid through an opening of diameter D_{ori} (Lugt, 1983, gives many examples which illustrate the diversity of situations in which vortex rings can be encountered). Viscous diffusion of the momentum contained in the vortex ring core causes the ring diameter to grow, with ambient fluid being engulfed, or entrained, into the core. The total circulation then decays, thereby decreasing the velocity of propagation of the ring. This decaying process leads to eventual anihilation of all vorticity initially contained in a vortex ring.

Flow visualization of vortex rings of varying strength, i.e., circulation, identifies the modes in which these can occur. At the low end of initial strengths, vortex rings display a smooth toroidal surface. As the initial strength increases, low amplitude azimuthal waves are displayed around the toroid. Further increase of the initial circulation is translated into vortex-ring matter being shed into the surrounding fluid, forming a trailing wake the extent of which increases with increase in initial vortex ring circulation. At the high end of initial strength, a well defined torodial shape is no longer observed after the rollup process. Instead, a blob of fluid moves forward which sheds appreciable quantity of fluid into a trailing wake where smaller scale vortical structures can be distinguished. Eventually, a well defined vortex ring emerges from the blob and keeps moving forward.

Vortex rings are classified in the literature as either laminar or turbulent. The following provides an overview of the currently available data which are, in general, only of a qualitative nature.

Maxworthy (1972) defines the bubble[1] Reynolds number

$$Re_0=\frac{U_0 D_0}{\nu} \tag{1}$$

[1] Some authors use the term bubble based on the idea that the shape of the fluid mass that moves forward is actually that of a bubble, and not a ring

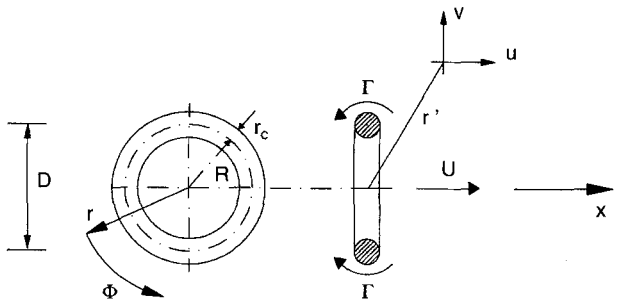

Fig. 1. Vortex ring – features and terminology

where U_0 is the initial velocity of translation of the bubble and D_0 is the bubble initial diameter.

He found experimentally that:

- for $Re_0 < 600$ the rings are stable (laminar);
- for $Re_0 > 600$ the rings develop azimuthal waviness;
- for $Re_0 > 1000$ upon completion of the rollup, flow breaks into turbulent motion (i.e., only a blob is seen), from which a new ring later emerges.

Sallet and Widmayer (1974) showed that hot-wire velocity traces of laminar vortex rings are smooth, while those of turbulent vortex rings displayed the same basic pattern but with high frequency low amplitude fluctuations superimposed. The position at which these traces were obtained is not stated. However, evidence gathered in the present work indicates that the traces must have been obtained outside the vortex ring core.

The behaviour of the ring seems to depend on the geometry of the ring generator. For instance, Auerbach (1988) found that vortex rings ejected from an orifice entrain less fluid than those ejected from a sharp-edged tube, and that the former also move faster. He also concludes that ring vortices generally go through four phases in their development: generation, laminar, "wavy", and turbulent, but leaves unexplained the fact that the distances (length) taken to the end of the laminar and to the end of the wavy phases are equal, irrespective of the generating parameters.

A looped vortex, such as a vortex ring induces its own motion as well as that of the surrounding fluid. Using the Biot-Savart law, and referring to Fig. 1, one finds for the velocity induced at the intersection of the ring plane with the axis along which it moves, i.e. $x = r = 0$:

$$u = \frac{\Gamma}{2R} \tag{2}$$

More generally, the induced velocity of a point located on the ring axis at a distance x from the ring is given by:

$$u_a = \frac{\Gamma}{2R} \frac{1}{(1 + x^2/R^2)^{3/2}} \tag{3}$$

Determination of the flow field induced in the vicinity of a vortex ring should, however, take into account the viscous effects of the fluid. These will dictate how fast the induced velocity, as calculated by Eq. (3), is achieved, and if it is achieved at all.

The vortex ring moves with a velocity of its own. Lamb (1945) took into account the core size to write, for a circular vortex ring of small cross-section in an ideal fluid:

$$U = \frac{\Gamma}{4\pi R} \left\{ \ln \left(\frac{8R}{r_c} \right) - \frac{1}{4} \right\} \tag{4}$$

This result applies to the case when the vorticity in the core is uniformly distributed. Later, Fraenkel (1970) and Saffman (1970) considered an arbitrary vorticity distribution across the core and Saffman (1970), including also the effect of viscosity, ended up with:

$$U = \frac{\Gamma}{4\pi R} \left\{ \ln \left(\frac{8R}{\sqrt{4\nu t}} \right) - 0.558 \right\} \tag{5}$$

Tung and Ting (1967) obtained what was subsequently shown to be the same result by employing a boundary-layer-type solution. The derivation of the same equation by two different methods seems to validate it. However, no experimental confirmation has so far been reported in the literature.

Against this background of known information, it is clear that there are several questions pertaining to the dynamics of a single vortex ring which are still unanswered, or are only partially answered at this stage. Accordingly, attention is focussed on the generation and decay of single viscous vortex rings, and to explore and explain as far as possible the following points:

- What is the exact meaning of the adjectives "laminar" and "turbulent" when applied to vortex rings?
- What is the actual decay of the velocity of a vortex ring? Is it the same for laminar and turbulent rings? Is Saffman's equation (Eq. (5)) a good model? What is its range of application?

The experiments (Dziedzic 1994) were conducted in the fluid mechanics laboratory of the Department of Mechanical Engineering at the University of Toronto.

3 Experimental apparatus

The vortex rings studied were generated in air, inside a cubical wooden chamber measuring 2.40 m on edge which minimizes the influence of ambient currents. The vortex generator, or vortex gun, consisted basically of a container and a driver. The container was an acrylic plastic box, and the driver either a loudspeaker, or compressed air released through a fast-action solenoid valve. Figure 2 shows the three different vortex guns employed. Even though the vortex guns allowed the use of interchangeable face plates, and different orifice sizes, it was found that the orifice size for which well defined vortex rings could be generated under the widest range of initial conditions was 2 cm. This, in turn, was probably determined by the size of the generator itself. Thus, $D_{ori} = 2$ cm for all cases.

The amplitude of motion of the loudspeakers could be controlled electronically, thus enabling the generation of vortex rings of different strengths. The same effect could be achieved by regulating the pressure of the compressed air discharged by the solenoid valve.

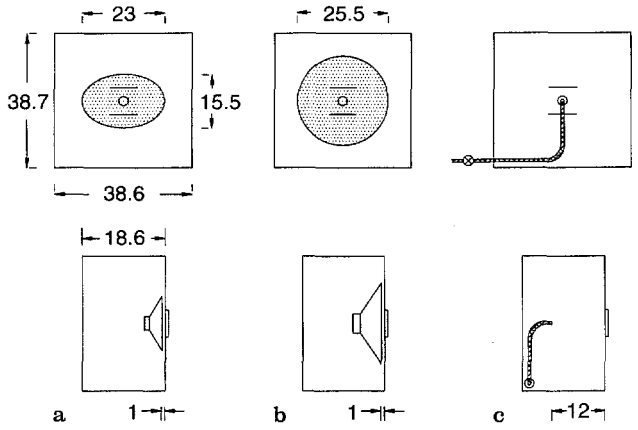

Fig. 2a–c. Frontal and side view of the three variations of vortex-ring generator used. a driver is a small loudspeaker; b driver is a large loudspeaker; c compressed air is release through a fast solenoid valve. All dimensions are in centimeters, and $D_{ori} = 2$ cm

Flow visualization was achieved by filling the generator box with a light paraffin oil mist. Generation, growth and decay of the vortex rings were recorded on video and by still photography. Prior to experiments, a grid was placed in the plane of travel of the vortex ring and the image recorded. This eliminated the problem of parallax and provided an accurate scale for data interpretation. However, the information obtained through the analysis of the captured images was of a gross nature and, in order to look into finer details of the motion, hot-wire anemometry was used to measure the instantaneous velocity of the fluid.

For that purpose, a DISA P14 single-wire probe was used in conjunction with an anemometer model 55M equipped with a 55M10 standard bridge. The platinum-plated tungsten wire was 1.25 mm long and had a diameter of 5 μm. For reasons of optimum sensitivity, the DISA 55M was operated at an overheat ratio of 1.8.

Since the magnitude of the velocities being measured was usually below 1.0 m/s, the standard hot-wire calibration techniques could not be employed. In lieu, the hot-wire probe was secured to a turntable of adjustable angular velocity. The radial position of the probe could also be varied which provided a wide range of calibration velocities. A detailed investigation of the pumping effect of the turntable and its influence on the velocity actually measured was conducted, and the significance of the disturbances caused by the residual wake left by the probe and its support was also examined (Dziedzic, 1994).

It should be noted that during velocity measurements with a hot-wire probe no smoke was utilized in order to prevent contamination of the instrument.

Recording of hot-wire data was carried out by an A/D board (PCL-812) connected to a 486/33 MHz PC-compatible computer. The hot-wire signal was conditioned before being digitized in order to make use of the full voltage band provided by the board, which recorded input between −5 V and +5 V and had an accuracy of 12 bits.

4 Results

4.1 Overview

Already during the early stages of the experimental study it was observed that varying the settings of the vortex ring generator would yield vortices with different characteristics. In particular, and essentially confirming the findings of earlier investigators, the types of vortex rings generated could be visually classified into three categories, viz., smooth, wavy, and rough, the order corresponding to increasing power at the generator (voltage applied to the loudspeaker, or pressure of the compressed air). What appeared to be laminar rings displayed a smooth toroidal shape, while turbulent ones had a rough surface and deposited fluid into a trailing wake. In the intermediary state, vortex rings exhibited surface instability in the form of azimuthal waves.

Despite all the attention given to vortex-ring-related research in the recent past, a definite classification of these structures based on flow properties could not be found in the literature. That is, one cannot state, based on the evidence available, whether the velocity field of a seemingly "turbulent" vortex ring is actually turbulent. Sallet and Widmayer (1974) presented hot-wire velocity traces of "laminar" and "turbulent" vortex rings, but restricted their measurements to the wake region, while making no mention of velocity measurements in the vortex ring core for the same cases. The question that immediately arises is: is the velocity in the core also turbulent? If not, could the vortex ring be properly called turbulent, or should it be termed turbulence-generating, instead? Also, would vortex rings generated with different experimental arrangements display signs of turbulence at, say, the same Reynolds number?

In order to resolve these issues, a detailed experimental program was carried out which involved video-taping and photographing the vortex rings generated with three different setups, viz. two loudspeakers of different sizes, and compressed air released through a fastacting solenoid valve. Evidence gathered also included velocity measurements by hot-wire anemometry of the vortex ring core and wake, and of the velocity distribution at the orifice.

Thus, three different setups were employed, all of which consisted of a variation of the orifice type. First, a small loudspeaker was mounted inside the plastic box. Second, the small loudspeaker was replaced by a large loudspeaker. Finally, the loudspeaker was removed and a compressed-air hose, connected to a fast-acting solenoid valve, positioned inside the plastic box, attached to the back wall and centered behind the orifice. Figure 2 shows these three variations and the dimensions involved.

When a loudspeaker is utilized its membrane can be made to move towards the orifice, or away from it. In both cases a vortex ring is generated, the explanation for the latter case being that air is pushed towards the back of the plastic box. The fluid then moves around the loudspeaker and is discharged through the orifice. For each of the three cases, a wide range of flow conditions was covered which correspond to the generation of smooth to rough vortex rings.

It should be noted that smooth rings are formed when the lowest settings are applied, viz., voltage applied to the speakers, or pressure difference across the valve, while rough vortex rings are generated at higher settings. In other words, rough vortex rings exist at higher energy levels than smooth ones. Therefore, if a ring is ever to appear rough, it will be so right after its formation, after which time it decays toward a smooth one. Auerbach (1988) and Liess and Didden (1976) suggest that a vortex ring will evolve from "laminar" into "turbulent", which was not observed in the present work.

Also, at higher settings usually more than one vortex ring will be formed by the roll up of the shear layer. That may be due to the fact that the rolled up portion of the layer, i.e., the vortex ring, achieves a velocity which is greater than that of the shear layer, thereby detaching itself from the shear layer, or, more likely, due to the occurrence of more than one velocity peak at the orifice during discharge due to pressure wave reflections inside the vortex gun. However, when a loudspeaker is employed, the portion of the membrane not parallel to the orifice plane may give rise to secondary, and tertiary, shear layers which will form vortex rings that travel along paths at an angle with the axis x as defined in Fig. 1. Measurements of the velocity profiles at the orifice plane for each case studied not only confirms the statements above, but also provide the specific initial conditions characterizing the experiments (Dziedzic 1994).

A summary of the vortex rings generated follows. Utilization of the terms laminar and turbulent is avoided, due to the lack of a formal definition. For the lowest settings, vortex rings will exhibit a smooth toroidal surface. As the settings are increased, first low amplitude azimuthal waves are noticed around the toroid. Further increase induces the occurrence of high amplitude waves and deposition of ring matter into a trailing wake. For even higher settings, azimuthal waves are no longer discernible, and the ring surface assumes a rough appearance. The vortex rings are characterized by their Reynolds number

$$Re = \frac{UD}{\nu} \tag{6}$$

- Small loudspeaker (s): nine voltage settings were employed, with both forward (toward the orifice) and backward motion of the loudspeaker membrane considered. For instance, case slf corresponds to: small loudspeaker with the lowest voltage setting (1) applied and the membrane moving forward. The Reynolds number of the vortex rings generated ranged from 400 to 5350, with azimuthal waves first being detected at $Re = 800$, and surface roughness at $Re = 1900$.
- Large loudspeaker (1): six voltage settings were employed, with both forward (toward the orifice) and backward motion of the loudspeaker membrane considered. The Reynolds number of the vortex rings generated ranged from 850 to 2950, with azimuthal waves first being detected at $Re = 1050$, and surface roughness at $Re = 1250$.
- Compressed air released through a solenoid valve (p): seven pressure settings were employed. The Reynolds number of the vortex rings generated ranged from 800 to 1850, with azimuthal waves first being detected at $Re = 1300$, and surface roughness at $Re = 1500$.

Photographs of some of the vortex rings studied are presented next which should clarify the terminology employed.

4.2
A tentative classification scheme emerges

Once a qualitative description of the flow conditions was obtained, quantification of the flow parameters was sought. To that end, hot-wire velocity measurements were carried out in order to determine the nature of the velocity distribution in the vortex ring core and in the fluid surrounding the vortex ring.

In the following, typical hot-wire velocimetry traces are presented for a wide range of flow conditions for each of the three experimental setups employed. For each case, hot-wire traces of the velocity, both inside and outside the vortex ring core are displayed. In addition, the maximum value of the vortex ring Reynolds number is listed, which occurs just after the vortex ring has been formed. The diameter and velocity of the vortex ring are determined from video sequences, in which ring diameter and position are measured directly from a TV screen. For the photographs shown, the vortex ring is positioned only a few orifice diameters away from the generator, and any sign of instability can be seen on the ring in the form of waviness or roughness, or by the presence of a trailing wake. The side-view photographs show rings travelling on a vertical plane and away from the orifice. The inclined view photographs were taken with the camera positioned in front of the vortex gun, but not aligned with the path of the moving ring. Photographs are printed to show the vortex ring moving from left to right.

Figure 3 shows schematically the position of the hot-wire probe relative to the vortex ring for the two types of trace depicted. It should be noted, however, that when velocity measurements are made with the hot-wire probe, no means of flow visualization are employed. For the first case (1), the probe is positioned along the x-axis passing through the center of the orifice, and for the second case (2) the probe is initially positioned at a radial position suggested by flow visualization and moved at 1 mm intervals, in a trial-and-error fashion, until the velocity trace indicates that the core of the vortex ring has passed over the wire. The frontal view of the vortex ring shows, in an exaggerated scale, the position and orientation of the sensing wire.

Figure 4 is a side-view photograph of a vortex ring with $Re = 400$. This close-up clearly shows the rolled-up structure of the ring core. Even though an inclined view is not shown (since this ring travels only a few centimeters and, when photographed, still has the orifice plate in the background) it was observed that its surface is smooth. Figure 5a displays the

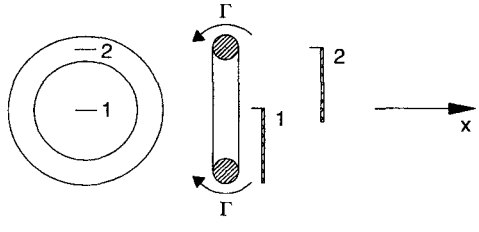

Fig. 3. Position of hot-wire probe while measuring velocity at the center-line (*1*) and velocity in the core (*2*)

Fig. 4. Photograph of vortex ring generated with setting s1f. $Re=400$

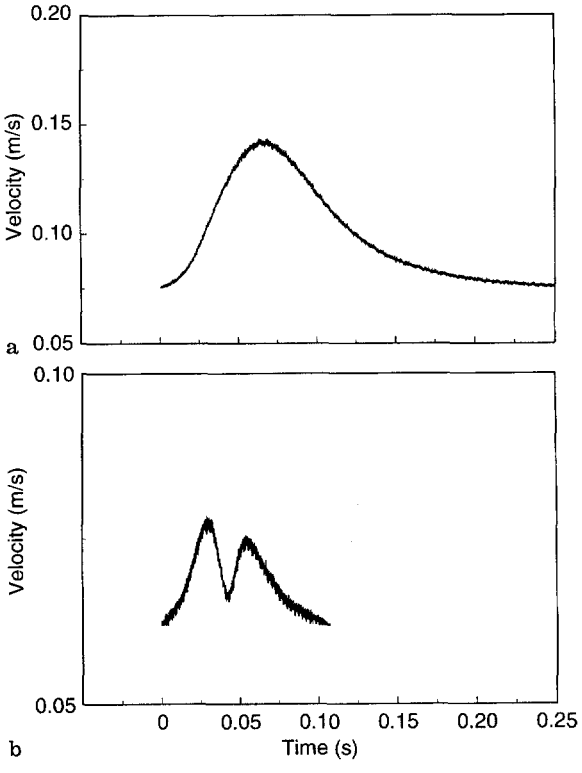

Fig. 5a,b. Hot-wire traces of velocity for vortex ring generated with setting s1f. **a** probe positioned on x-axis; **b** vortex ring core passing over the probe. $Re=400$

velocity signal on the axis of travel of the ring, i.e., its x-axis, (henceforth simply termed the center-line signal), while Fig. 5b displays the velocity signal obtained when the hotwire probe is positioned in the path of travel of the ring core (from now on simply termed the core signal). The velocity displayed in these plots is the magnitude of the velocity vector, as measured by the hot-wire probe ($|\mathbf{q}|=\sqrt{u^2+v^2+w^2}$, where u, v and w are the cartesian components of the velocity vector $\mathbf{q}$.). The lowest point between the peaks corresponds to the velocity at which the vortex ring travels, while the peaks are due to the rotating motion in the core. With the probe positioned at (2) as depicted in Fig. 3, the velocity components are as follows: u increases as the ring approaches the probe and reaches a maximum when the center of the core passes over the probe, then decreases as the ring moves away from the probe (the maximum value is the velocity of propagation of the vortex ring, U): v is negligible outside the core, zero at the center of the core, and has a sinusoidal distribution inside the core, being positive in the first half and negative in the second half of the core: w is negligible. Since the direction of the v-component cannot be identified with the hot-wire setup utilized, all v-values are sensed as positive, and a double-peaked trace is generated which is due to the sum of the u and $|v|$ components. The amplitude of the two peaks displayed may not be the same because the exact center of the core is not passing over the probe, or because the ring may be travelling at an angle with the x-axis centered at the orifice and normal to the generator. Identical scaling is not applied to all of the plots, since the intention here is to stress the existence or the absence of a turbulent component in the signal. Also, the origin of time is not common to all plots, but merely indicates when the influence of each travelling ring was first sensed by the hot-wire probe. For the case considered in Figs. 4 and 5, none of the hot-wire signals exhibit a turbulent component and, hence, it seems plausible to call them laminar. The high frequency component displayed is due to the utilization of a data acquisition rate which was sensitive to electronic noise.

Figure 6 presents a side-view as well as an inclined-view photograph of a vortex ring with $Re=1050$, a second and a third vortex rings are also shown. Low amplitude azimuthal waves can be seen. In Fig. 6 the lead vortex ring travels along the centerline of the orifice (not shown). The second and third rings follow a curved path due to jet deflection. This is of little concern here since attention is focused on the lead ring only. Regarding the density of the mist, measurements coupled with calculations showed that oil accounts only for 0.0004% of its total volume, and thus, density is that of the air in the chamber. Figure 7a displays the center-line signal, and Fig. 7b displays the core signal, both still laminar.

Figure 8 presents a side-view as well as an inclined-view photograph of a vortex ring with $Re=1650$. A rough toroidal surface and trailing wake can be seen. Figure 9a displays the center-line signal, and Fig. 9b displays the core signal, now both turbulent. It should be noticed that turbulence is present over the full extent of the wake. When a puff of smoke, rather than an actual ring, is formed, determination of ring diameter and ring position becomes, at best, arbitrary. The approach taken was to use the maximum diameter of the puff or bubble, and the position of its front as the relevant "ring" values. This fact is reflected in the observation that the Reynolds number varies rather erratically whenever the photographs show a puff of smoke.

Based on the evidence collected, it is now possible to propose a classification for vortex rings:

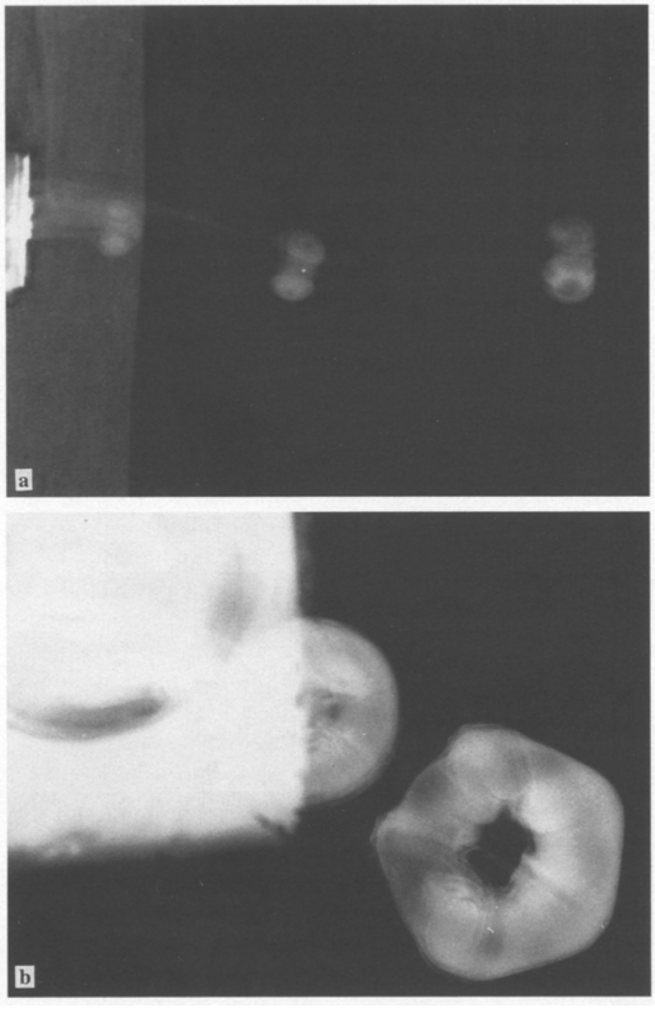

Fig. 6. Side view **a** and inclined view **b** photographs of vortex ring generated with setting l2f. $Re = 1050$

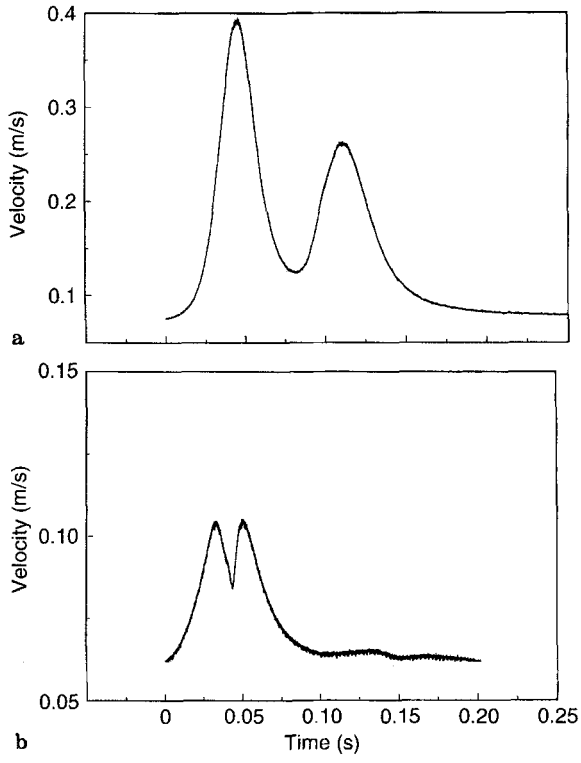

Fig. 7a,b. Hot-wire traces of velocity for vortex ring generated with setting l2f. **a** probe positioned on x-axis; **b** vortex ring core passing over the probe. $Re = 1050$

- Laminar vortex rings are those which have a smooth appearance, a laminar core, and a laminar wake.
- Wavy vortex rings are those which exhibit azimuthal waves, a laminar core, and a laminar wake.
- Turbulence-producing vortex rings are those which exhibit a rough surface, a laminar core, and a turbulent wake.
- Turbulent vortex rings are puffs, with a turbulent core, and a turbulent wake.

Prediction of vortex ring instability based on its Reynolds number seems to be possible, at least approximately, if one considers the data gathered. Waviness was first observed for a Reynolds number of 800, 1050, and 1300, respectively, for vortex rings generated with the small loudspeaker, large loudspeaker, and compressed air setup. Turbulence, be it in the ring core or in the wake, was detected at Reynolds numbers of 2300, 2500, and 1650, respectively. Given the uncertainty associated with critical Reynolds numbers of other flow situations, it appears reasonable to conclude that *waviness* occurs, approximately, at $Re \simeq 1000$, and *turbulence* occurs, approximately, at $Re \simeq 2000$. No critical Reynolds number is proposed which would definitively separate turbulence-producing rings from turbulent rings. Apparently, there is none; rather, the difference seems to rest in the nature of the generating jet (see also Dziedzic and Leutheusser 1994) as indicated by measurements of the velocity profile at the orifice plane (Dziedzic 1994). These measurements show that turbulent rings result when a turbulent jet emerges from the vortex gun.

Table 1 presents a summary of the features of the vortex rings generated with all experimental setups. For each case are listed Reynolds numbers (unrounded), the initial appearance of the vortex ring, the existence or absence of a trailing wake, and the type of velocity signal measured in the core and at the center-line (cf. laminar or turbulent), with the rms of the middle and high-frequency components of the signal enclosed in parentheses. Determination of these values by spectral analysis generally substantiate[2] the visual classification of the signals, with the turbulent rms being significantly larger than the laminar rms.

4.3 Vortex-ring decay

Saffman's Eq. (5) cannot be applied to the full duration of motion of a vortex ring without knowledge of $\Gamma(t)$ and $R(t)$. When Saffman (1970) obtained Eq. (5), he employed Hamel-Oseen's solution for the viscous decay of a vortex line, viz.

$$\Gamma = \Gamma_0(1 - \exp[-r_c^2/4\nu t]) \tag{7}$$

[2]Question marks indicate the cases where the calculated value of the rms seems not to corroborate visual observations

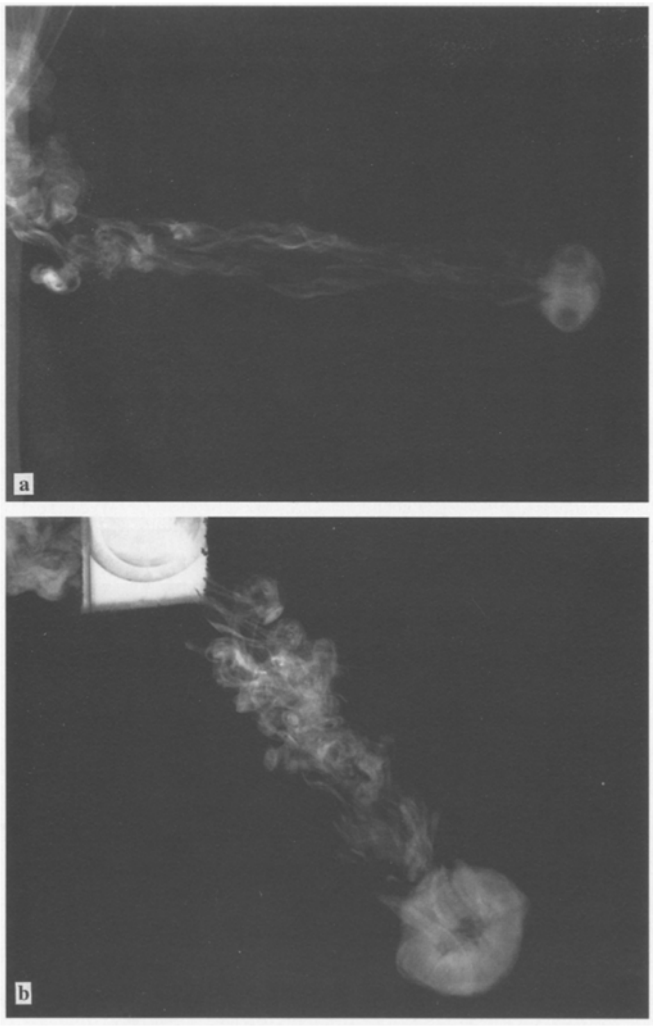

Fig. 8. Side view **a** and inclined view **b** photographs of a vortex ring generated with setting p5. $Re = 1650$

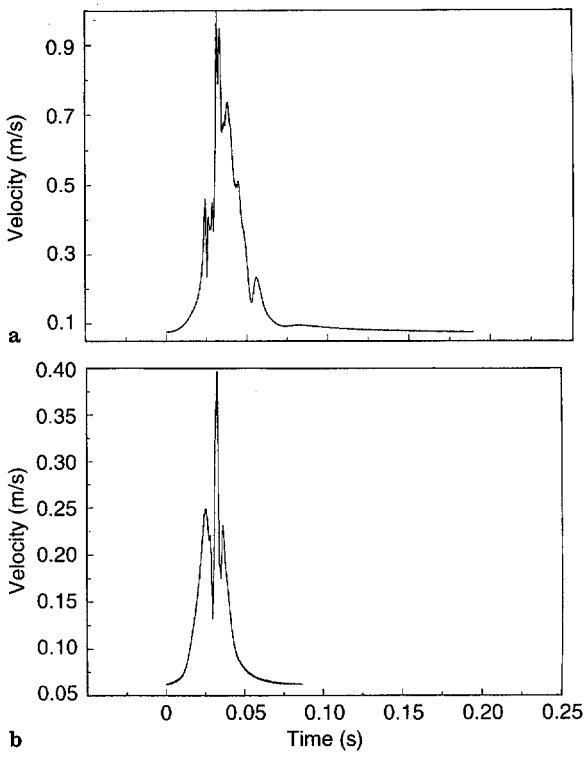

Fig. 9a,b. Hot-wire traces of velocity for vortex ring generated with setting p5. **a** probe positioned on x-axis; **b** vortex ring core passing over the probe. $Re = 1650$

which can be used here if one assumes that the ratio r_c/R remains constant throughout the motion of the vortex ring and Γ_0 is calculated from Eq. (4). The assumption of constant r_c/R is justified by the present observations as well as those of Johnson (1970). Vortex-ring core radii determined from velocity signals range from 0.08 to 0.35 cm (Dziedzic 1994), which correspond to values of R/r_c between 3.5 and 10. The problem of determining $R(t)$ can be circumvented by simply using experimental data.

However, it would clearly be more useful if the decay of a vortex ring, i.e., the decrease of its Reynolds number with time or distance travelled, could be predicted based solely on the initial conditions of motion. To that end, one can use the hydrodynamic impulse M of a vortex ring, i.e.,

$$M = \rho\pi R^2 \Gamma = \text{constant} \tag{8}$$

to update R, since it has been pointed out by Saffman (1970) and Shariff and Leonard (1992) that the hydrodynamic impulse is conserved in the absence of body forces even if viscous stresses are included in the equation of motion.

Three different models were tested for the calculation of $Re(t)$. They are:

I. Determine Γ_0 with Kelvin's Eq. (4); determine t_0 with Saffman's Eq. (5); update circulation with Hamel-Oseen's Eq. (7); use experimental data for $R(t)$.

II. Determine Γ_0 with Kelvin's Eq. (4); determine t_0 with Saffman's Eq. (5); update circulation with Hamel-Oseen's Eq. (7); assume conservation of the hydrodynamic impulse and update R with

$$R_t = R_{t-\Delta t} \frac{\Gamma^2_{t-\Delta t}}{\Gamma^2_t} \tag{9}$$

III. Determine Γ_0 with Kelvin's Eq. (4); determine t_0 with Saffman's Eq. (5); use experimental data for $R(t)$; assume conservation of the hydrodynamic impulse and update Γ with

$$\Gamma_t = \Gamma_{t-\Delta t} \frac{R^2_{t-\Delta t}}{R^2_t} \tag{10}$$

Position x is updated by adding $U\Delta t$ at every time interval for all cases.

In the present case Δt was made equal to 1/30 s in all calculations to render the performance of the three models comparable, since experimental data were only available at 1/30 s intervals. Figures 10–13 show the variation of the vortex ring Reynolds number with time and distance travelled for a few of the cases studied.

In the figures symbols represent experimental data points, a solid line is a least-squares exponential fit (suggested by the fact that data plots of Re versus x' or t' in a double-logarithmic scale are approximated very well by a straight line), a dotted

Table 1. Summary of experimental findings for all setups. $Re = UD/\nu$, "surface" indicates the visual appearance of the vortex ring; "wake" indicates the presence or absence of a trailing wake; "core" and "c-line" indicate whether the velocity signal measured, respectively, in the core and at the center-line is laminar or turbulent. The rms of the middle and high-frequency components of the signal are enclosed in parenthesis.

Settings	Re	Surface	Wake	Core (rms)	c-line (rms)
s1f	391	smooth	no	laminar (0.38)	laminar (0.10)
s1b	391	smooth	no	laminar (0.55)	laminar (0.16)
s2f	555	smooth	no	laminar (0.28)	laminar (0.27)
s2b	647	smooth	no	laminar (0.46)	laminar (0.13)
s3f	555	smooth	no	laminar (0.37)	laminar (0.31)
s3b	797	wavy	yes	laminar (0.49)	laminar (0.30)
s4f	924	smooth	yes	laminar (0.21)	laminar (0.57)
s4b	1281	wavy	yes	laminar (0.16)	laminar (0.77)
s5f	996	wavy	yes	laminar (0.17)	laminar (0.74)
s5b	1666	wavy	yes	laminar (0.16)	laminar (0.31)
s6f	1096	wavy	yes	laminar (0.51)	laminar (0.64)
s6b	1890	wavy	yes	laminar (0.27)	laminar (0.22)
s7f	1923	rough	yes	laminar (0.16)	laminar (0.44)
s7b	2277	rough	yes	laminar (0.14)	turbulent (9.49)
s8f	2660	rough	yes	laminar (1.02?)	laminar (1.61?)
s8b	3585	rough	yes	laminar (1.28?)	turbulent (2.21)
s9f	1709	rough	yes	laminar (0.70)	laminar (2.54?)
s9b	5337	rough	yes	laminar (0.77)	turbulent (2.92)
l1f	827	smooth	no	laminar (0.50)	laminar (0.05)
l1b	732	smooth	no	laminar (0.65)	laminar (0.16)
l2f	1056	wavy	yes	laminar (0.45)	laminar (0.17)
l2b	927	wavy	yes	laminar (0.27)	laminar (0.11)
l3f	1356	wavy	yes	laminar (0.35)	laminar (0.27)
l3b	NA	wavy	yes	laminar (0.35)	laminar (0.31)
l4f	1263	rough	yes	laminar (0.24)	laminar (0.56)
l4b	2509	rough	yes	laminar (0.86)	turbulent (0.64?)
l5f	1286	rough	yes	laminar (0.60)	laminar (0.19)
l5b	2440	rough	yes	laminar (1.16?)	turbulent (1.00?)
l6f	1269	rough	yes	laminar (0.41)	turbulent (5.11)
l6b	2928	rough	yes	laminar (0.75)	turbulent (2.18)
p1	817	smooth	no	laminar (0.79)	laminar (0.75)
p2	1280	wavy	yes	laminar (0.74)	laminar (0.28)
p3	1512	rough	yes	laminar (1.31?)	laminar (1.64?)
p4	1621	rough	yes	laminar (1.68?)	laminar (0.80)
p5	1636	rough	yes	turbulent (3.50)	turbulent (2.13)
p6	1835	rough	yes	turbulent (2.67)	turbulent (4.43)
p7	1792	rough	yes	turbulent (3.48)	turbulent (8.84)

line is obtained with model I, a dot-dashed line is obtained with model II, and a dashed line is obtained with model III.

It is evident that all three models yield good results. However, it is the more useful model II which offers itself as the preferable choice. The "wiggles" in the curves obtained with models I and III are due to the use of measured data values for R. The "wiggles" in the curves obtained with model II are due to the use of a relatively large Δt (1/30 s) and should disappear when the time step is reduced.

Alternative models for the calculation of circulation, such as those proposed by Glezer and Coles (1990) and Liess and Didden (1979), were tested, but yielded unsatisfactory results.

An additional test was carried out to test the usefulness of the model proposed. In particular, the total distance travelled by a vortex ring was experimentally determined, and Eq. (5)

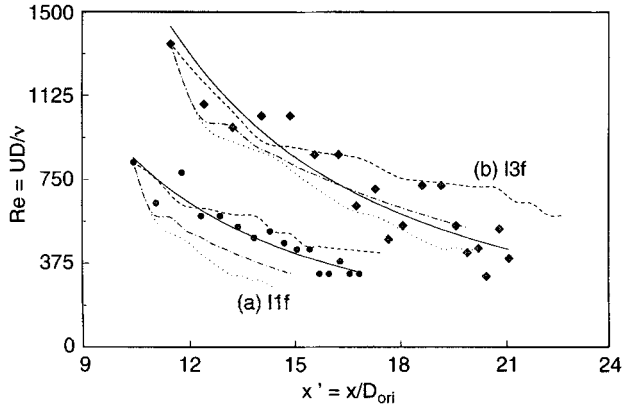

Fig. 10. Variation of vortex ring Reynolds number with distance travelled for cases l1f ($Re = 850$) and l3f ($Re = 1350$). Symbols are experimental data points, a solid line is an exponential fit, a dotted line is obtained with model I, a dot-dashed line is obtained with model II, and a dashed line is obtained with model III

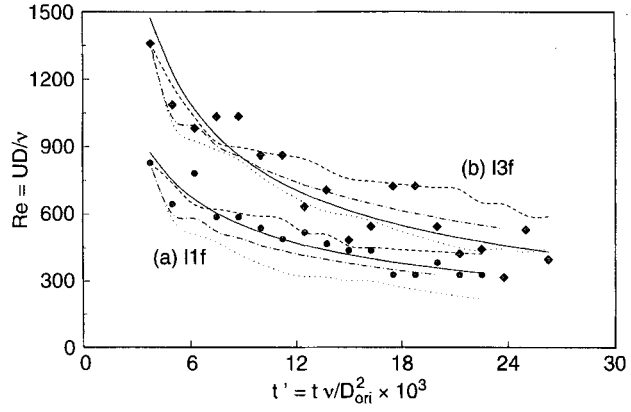

Fig. 11. Variation of vortex ring Reynolds number with time for cases l1f ($Re = 850$) and l3f ($Re = 1350$). Symbols are experimental data points, a solid line is an exponential fit, a dotted line is obtained with model I, a dot-dashed line is obtained with model II, and a dashed line is obtained with model III

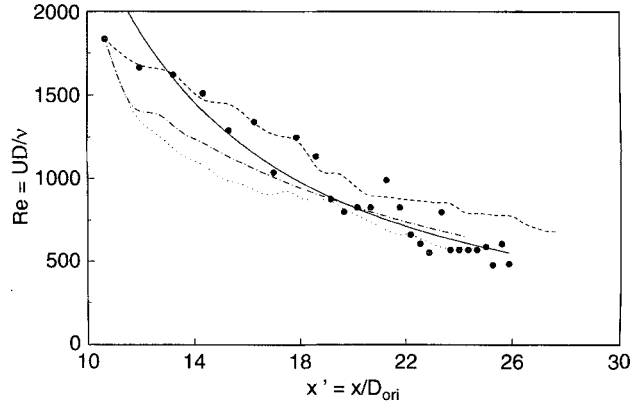

Fig. 12. Variation of vortex ring Reynolds number with distance travelled for case p6 ($Re = 1850$). Symbols are experimental data points, a solid line is an exponential fit, a dotted line is obtained with model I, a dot-dashed line is obtained with model II, and a dashed line is obtained with model III

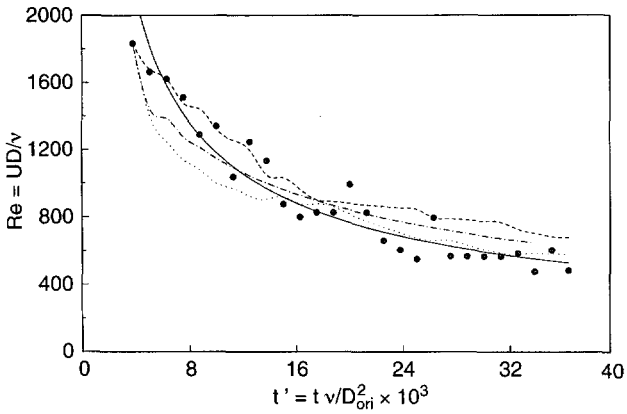

Fig. 13. Variation of vortex ring Reynolds number with time for cases p6 ($Re = 1850$). Symbols are experimental data points, a solid line is an exponential fit, a dotted line is obtained with model I, a dot-dashed line is obtained with model II, and a dashed line is obtained with model III

Table 2. Maximum distance travelled by a vortex ring. Setting refers to the experimental setup employed, Re is the vortex ring Reynolds number, $x_{max,meas}$ is the measured distance, $x_{max,theo}$ is the theoretical distance, and error is the relative error defined as $(|x_{max,meas} - x_{max,theo}|/x_{max,meas}) \times 100$

Settings	Re	$x_{max,meas}$ (cm)	$x_{max,theo}$ (cm)	Error (%)
s1f	391	12.6	11.6	7.9
s1b	391	10.7	11.9	11.2
s2f	555	15.4	17.9	16.2
s2b	648	21.1	21.0	0.5
s3f	555	18.3	19.0	3.8
s3b	797	26.7	25.9	3.0
s4f	926	27.7	29.6	6.9
s4b	1210	44.7	45.8	2.5
s5f	997	31.5	34.6	9.8
s5b	1666	54.1	64.9	20.0
s6f	1096	33.4	38.6	15.6
s7f	1922	59.8	64.7	8.2
l1f	827	25.6	27.1	5.9
l1b	732	25.6	25.2	1.6
l2f	1056	37.4	36.8	1.6
l2b	928	40.8	34.8	14.7
l3f	1357	40.0	46.6	16.5
l4f	1264	44.2	46.4	5.0
l5f	1287	44.2	39.4	10.9
p1	818	34.2	29.0	15.2
p2	1280	48.8	47.3	3.1

was employed to calculated its theoretical value from

$$x_{max} - x_0 = \int_{t_0}^{t=\infty} U\,dt = \int_{t_0}^{t=\infty} \left\{ \frac{\Gamma}{4\pi R} \left\{ \ln\left(\frac{8R}{\sqrt{4\nu t}} \right) - 0.558 \right\} \right\} dt \tag{11}$$

Analytical integration of this is possible if the observed linear growth rate is applied to R, Hamel-Oseen's solution for the viscous decay of circulation (Eq. (7)) is used, and if one assumes that $r_c/R = \text{constant}$. However, the resulting function would be in the form of an infinite series and would be of an approximate nature. For this reason, it was decided to numerically integrate equation 11, employing model II with $\Delta t = 0.001$ s.

Computations were carried out while the velocity U of the vortex ring remained above 0.0001 m/s. Results are shown in Table 2. This shows that the relative error between experimental and theoretical values is not excessive in most cases. Thus, it would appear that Saffman's Eq. (5) can, indeed, be considered to be experimentally substantiated. Saffman (1993) indicated not being aware of the existence of prior experimental confirmation of his model.

Finally, it may be noted that the vortex rings considered herein were not particularly thin, which did not seem to affect the performance of Saffman's equation. Also, Eq. (5) shows good agreement even with the observed behaviour of turbulent rings. The latter is probably due to the fact that the level of turbulence was low in the rings examined. At the same time, however, it may also be true that higher levels of turbulence will obliterate any large core structure and, therefore, not allow a vortex ring to exist.

5 Conclusions

A tentative classification scheme for vortex rings is proposed based on experimental observations. It states that there are essentially four different types of vortex rings, viz., laminar, wavy, turbulence-producing, and turbulent. The distinction between laminar and wavy rings is merely visual, in the sense that the velocity signal in the vortex ring core and in the wake is laminar in both cases, but that azimuthal waves occur around the toroidal surface of a wavy ring. Data gathered during the present research work suggest that $Re \simeq 1000$ marks the transition between laminar and wavy vortex rings. Turbulence-producing vortex rings are those with a turbulent wake, while turbulent rings are those with a turbulent core and wake. Notwithstanding the likelihood that mode of generation may have some bearing on the value of the critical Reynolds number, present data indicate that above $Re \simeq 2000$ vortex rings will be turbulence-producing or turbulent. It is suggested that turbulent rings may only be formed when the fluid that rolls up to form the vortex ring already has turbulent velocity components prior to the roll-up process.

It must be remembered, however, that the proposed classification scheme, while appealing and well substantiated, is based on only a limited range of vortex generators. Therefore, further experiments are necessary in order to justify a claim of true generality for the present findings.

A thorough examination of models of vortex ring decay suggests that Saffman's Eq. (5) may be applied to all types of vortex rings, when it is used in conjunction with the Hamel-Oseen solution for the decay of circulation/vorticity (Eq. (7)), and conservation of hydrodynamic impulse is assumed and employed to update the value of the vortex ring diameter. Therefore, given the initial diameter and velocity of a vortex ring, it is then possible to predict its motion in a quiescent fluid in time and space with good accuracy.

References

Auerbach D (1988) Some open questions on the flow of circular vortex rings. Proc. IUTAM Symp. Fundamental Aspects of Vortex Motion, held in Tokyo, Japan, August 31–September 4/87. Fluid Dyn Res 3: 209–213

Didden N (1979) On the formation of vortex rings: rolling-up and production of circulation. J Appl. Math Phys (ZAMP) 30: 101–116
Dziedzic M (1994) An Experimental Study of Viscous Vortex Rings. PhD thesis, University of Toronto, Toronto, Canada
Dziedzic M; Leutheusser HJ (1994) Generation and Decay of Vortex Rings. Z Angew Math Mech (ZAMM) 74: 485–487
Fraenkel LE (1970) On steady Vortex Rings of Small Cross-section in an Ideal Fluid. Proc Royal Soc London 316: 29–62
Glezer A; Coles D (1990) An Experimental Study of a Turbulent Vortex Ring. J Fluid Mech 221: 243–283
Johnson GM (1970) Researches on the Propagation and Decay of Vortex Rings. United States Air Force, Aerospace Research Laboratories. ARL 70-0093, June 1970
Lamb Sir H (1945) Hydrodynamics. Dover Publications
Liess C; Didden N (1976) Experimente zum Einfluß der Anfangsbedingungen auf die Instabilität von Ringwirbeln. Z Angew Math Mech (ZAMM) 56: 206–208
Lugt HJ (1983) Vortex Flow in Nature and Technology. John Wiley & Sons–Interscience
Maxworthy T (1972) The Structure and Stability of Vortex Rings. J Fluid Mech 51: 15–32
Saffman PG (1970) The Velocity of Viscous Vortex Rings. Studies Appl Math XLIX: 371–380
Saffman PG (1993) Personal Communication, December 24
Sallet DW; Widmayer RS (1974) An Experimental Investigation of Laminar and Turbulent Vortex Rings in Air Z Flugwiss 22: 207–215
Shariff K; Leonard A (1992) Vortex Rings. Annual Rev Fluid Mech 24: 235–279
Tung C; Ting L (1967) Motion and Decay of a Vortex Ring. Phys. Fluids 10: 901–910